

# Analytical solution for electrolyte concentration distribution in lithium-ion batteries

Anupama Guduru · Paul W. C. Northrop ·  
Shruti Jain · Andrew C. Crothers · T. R. Marchant ·  
Venkat R. Subramanian

Received: 12 December 2011 / Accepted: 13 February 2012 / Published online: 1 March 2012  
© Springer Science+Business Media B.V. 2012

**Abstract** In this article, the method of separation of variables (SOV), as illustrated by Subramanian and White (J Power Sources 96:385, 2001), is applied to determine the concentration variations at any point within a three region simplified lithium-ion cell sandwich, undergoing constant current discharge. The primary objective is to obtain an analytical solution that accounts for transient diffusion inside the cell sandwich. The present work involves the application of the SOV method to each region (cathode, separator, and anode) of the lithium-ion cell. This approach can be used as the basis for developing analytical solutions for battery models of greater complexity. This is illustrated here for a case in which nonlinear diffusion is considered, but will be extended to full-order

nonlinear pseudo-2D models in later work. The analytical expressions are derived in terms of the relevant system parameters. The system considered for this study has  $\text{LiCoO}_2$ – $\text{LiC}_6$  battery chemistry.

**Keywords** Battery model · Analytical solution · Concentration distribution · Separation of variables method

## List of symbols

$a$	Specific interfacial area ( $\text{m}^2/\text{m}^3$ )
$B$ , Brugg	Bruggeman coefficient
$c_0$	Concentration at initial time $t = 0$
$c_i(x, t)$	Concentration in region $i$ ( $\text{mol}/\text{m}^3$ )
$C_i(X, \tau)$	Dimensionless concentration in region $i$
$D$	Diffusion coefficient of lithium ions in the electrolyte ( $\text{cm}^2/\text{s}$ )
$D_{\text{eff},i}$	Effective diffusion coefficient of the Li-ion in region $i$ ( $\text{cm}^2/\text{s}$ )
$F$	Faraday's constant ( $\text{C}/\text{mol}$ )
$i_{\text{app}}$	Applied current density ( $\text{A}/\text{m}^2$ )
$j_i$	Flux density of the Li-ions into the electrode in region $i$ ( $\text{mol}/\text{m}^2\text{s}$ )
$J_i$	Dimensionless flux density in region $i$
$l_i$	Thickness of region $i$ (m)
$K$	Ratio of dimensionless flux densities in the electrodes
$L$	Total thickness of cell (m)
$p$	Dimensionless position of positive electrode/separator interface
$q$	Dimensionless position of separator/negative electrode interface
$t$	Time (s)
$t_+$	Transference number
$x$	Position (m)
$X$	Dimensionless position

A. Guduru  
Department of Chemical Engineering, Tennessee Tech  
University, Cookeville, TN 38505, USA

## Present Address:

A. Guduru  
Bechtel Corporation, Houston, TX, USA

P. W. C. Northrop · V. R. Subramanian (✉)  
Department of Energy, Environmental and Chemical  
Engineering, Washington University, St. Louis, MO 63130, USA  
e-mail: vsubramanian@wustl.edu

S. Jain  
Department of Chemical Engineering, Indian Institute  
of Technology, Gandhinagar 380005, Gujarat, India

A. C. Crothers  
Department of Chemical and Biomolecular Engineering,  
North Carolina State University, Raleigh, NC 27695, USA

T. R. Marchant  
School of Mathematics and Applied Statistics, University  
of Wollongong, Wollongong, NSW 2522, Australia

$\alpha_n, \beta_n$	Eigenvalues
$\varepsilon_i$	Porosity in region $i$
$\tau$	Dimensionless time

## 1 Introduction

With the emergence of rechargeable Li-ion batteries in the consumer electronics, various mathematical models have been developed in order to focus on the optimization of the battery design. Isothermal and non-isothermal models were suggested by Gomadam et al. [1]. Doyle et al. [2–4] developed cell sandwich models for diffusion limitations and ohmic losses. Some models have incorporated many aspects which affect battery performance, such as porosity or mass transfer limitations when performing simulations [5–13]. Many efforts have explored methodologies to update these complicated models in order to make them simpler and more computationally efficient so as to better understand the behavior of these power systems during charging and discharging [14–20]. For example, computational efficiency is important in hybrid systems for control and management. In order to capture the essential features that characterize such behavior, analytical expressions for the variables in terms of dimensionless quantities can be found. The obtained expressions are useful for both design and performance testing of diffusion-limited lithium-ion batteries, under different operating conditions and scenarios.

The aim of the present work is to obtain analytical expressions for the concentration profile in a lithium-ion cell in terms of the relevant system parameters using the separation of variables (SOV) method. Because of the nature of the equations, a method developed in a previous work [21] is useful and efficient in finding the constants of integrations and coefficients. The solution obtained is validated by comparing the profiles found using this method to profiles from a numerical finite difference solution.

## 2 Model

The base unit of a Li-ion battery is a cell sandwich consisting of a positive and negative electrode with a separator as shown in Fig. 1. For simplicity, a 1D model is considered with the positive composite electrode ranging from  $x = 0$  to  $l_p$ , separator ranging from  $l_p$  to  $l_p + l_s$  and the negative composite electrode from  $l_p + l_s$  to  $l_p + l_s + l_n$ . The electrolyte phase is continuous across the cell domain, while the solid phase exists only in the electrode regions. Thus, the transport can be described in each of the three regions by a system of three partial differential equations coupled together at the interfaces  $x = l_p$  and at  $x = l_p + l_s$ . The dependent variables are the ionic concentration in both electrodes and the separator with respect to time and the position,  $x$ .

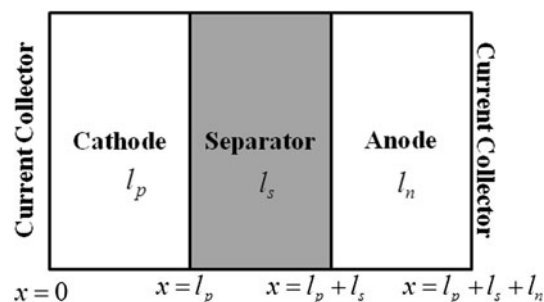


**Fig. 1** Schematic representation of the three regions in Li-ion cell

The governing equations for this model are based on Fick's law and accounts for diffusion in the electrolyte due to the concentration gradient as well as transfer of the lithium ions into and out of the electrolyte from the solid electrodes. For this article, only diffusion limitations in the electrolyte phase are considered and all other limitations are ignored. Note that the term  $K$  in (3) acts as a source (or sink) representing the ratio between the rates of transfer of lithium ions between the solid electrodes and liquid electrolyte during charging (or discharging). The governing equations for the positive electrode, separator, and the negative electrode are given, in dimensionless form, as Eqs. 1–3, respectively.

$$\frac{\partial C_1}{\partial \tau} = \varepsilon_p^{\text{Brugg}} - 1 \frac{\partial^2 C_1}{\partial X^2} \quad (0 \leq X \leq p, \text{ positive electrode}) \quad (1)$$

$$\frac{\partial C_2}{\partial \tau} = \varepsilon_s^{\text{Brugg}} - 1 \frac{\partial^2 C_2}{\partial X^2} \quad (p \leq X \leq q, \text{ separator}) \quad (2)$$

$$\frac{\partial C_3}{\partial \tau} = \varepsilon_n^{\text{Brugg}} - 1 \frac{\partial^2 C_3}{\partial X^2} + K \quad (q \leq X \leq 1, \text{ negative electrode}) \quad (3)$$

While the initial and boundary conditions (BC) are given as

$$C_1(X, \tau) = C_2(X, \tau) = C_3(X, \tau) = 0 \text{ at } \tau = 0 \quad (4)$$

$$-D \frac{\partial C_1}{\partial X} = 0 \text{ at } X = 0, \quad -D \frac{\partial C_3}{\partial X} = 0 \text{ at } X = 1 \quad (5)$$

$$\frac{\partial C_1}{\partial X} = \frac{\varepsilon_s^{\text{Brugg}}}{\varepsilon_p^{\text{Brugg}}} \frac{\partial C_2}{\partial X} \text{ at } X = p, \quad \frac{\partial C_2}{\partial X} = \frac{\varepsilon_n^{\text{Brugg}}}{\varepsilon_s^{\text{Brugg}}} \frac{\partial C_3}{\partial X} \text{ at } X = q \quad (6)$$

$$C_1(X, \tau) = C_2(X, \tau) \text{ at } X = p, \\ C_2(X, \tau) = C_3(X, \tau) \text{ at } X = q \quad (7)$$

A detailed derivation of these dimensionless equations is given in the [Appendix](#).

## 3 Solution technique

Several methods for obtaining the analytical solutions to this problem can be found in the literature, such as

perturbation techniques and Laplace transforms [22, 23]. The method of SOV is used here to determine the concentration at any point within the three regions of a Li-ion battery for constant current conditions at any time. These governing equations have analytical eigenfunction-value series solutions, which describe the galvanostatic discharge. The Li-ion cell sandwich is considered with a uniform current distribution. In order to obtain analytical solutions to address mass transfer limited situations in the electrolyte phase (as a worst case scenario), we assume that the pore wall flux of ions into and out of the electrode is constant for all time and across the entire electrode [24].

Following Subramanian and White [21], the following variable transformation is used to separate the transient solution and the steady state solution in the three regions.

$$C_i(X, \tau) = U_i(X, \tau) + W_i(X) + V_i(\tau) \quad \text{for } i = 1, 2, 3 \quad (8)$$

Here  $W_i(X)$  is the steady state solution which satisfies the source and sink terms in (1) and (3) representing the pore wall flux;  $V_i(\tau)$  satisfies the non-homogeneity arising when non-constant BCs are used; and  $U_i(X, \tau)$  describes the transient solution, which satisfies the homogenous BCs and governing equations, and  $i$  denotes the region of interest. By inserting Eq. 8 into Eqs. 1–3, we arrive at the following:

$$\frac{\partial U_1}{\partial \tau} + V_1'(\tau) = \frac{\varepsilon_p^{\text{Brugg}}}{\varepsilon_p} \left[ \frac{\partial^2 U_1}{\partial X^2} + W_1''(X) \right] - 1 \quad (9)$$

$$\frac{\partial U_2}{\partial \tau} + V_2'(\tau) = \frac{\varepsilon_s^{\text{Brugg}}}{\varepsilon_s} \left[ \frac{\partial^2 U_2}{\partial X^2} + W_2''(X) \right] \quad (10)$$

$$\frac{\partial U_3}{\partial \tau} + V_3'(\tau) = \frac{\varepsilon_n^{\text{Brugg}}}{\varepsilon_n} \left[ \frac{\partial^2 U_3}{\partial X^2} + W_3''(X) \right] + K \quad (11)$$

Since  $U_i(X, \tau)$  alone satisfies the homogeneous governing equations, the variables can be separated to give the following governing equations for  $U_i(X, \tau)$ , which are analogous across the three regions

$$\frac{\partial U_i}{\partial \tau} = \frac{\varepsilon^{\text{Brugg}}}{\varepsilon} \left[ \frac{\partial^2 U_i}{\partial X^2} \right] \quad \text{for } i = 1, 2, 3 \quad (12)$$

where the porosity,  $\varepsilon$ , in Eq. 12 represents the porosity in the  $i$ th region: i.e., either  $\varepsilon_p$ ,  $\varepsilon_s$ , or  $\varepsilon_n$ , as appropriate. Similarly,  $V_i(\tau)$  and  $W_i(X)$  will be related by:

$$V_1'(\tau) = \frac{\varepsilon_p^{\text{Brugg}}}{\varepsilon_p} [W_1''(X)] - 1 = A \quad (13)$$

$$V_2'(\tau) = \frac{\varepsilon_s^{\text{Brugg}}}{\varepsilon_s} [W_2''(X)] = P \quad (14)$$

$$V_3'(\tau) = \frac{\varepsilon_n^{\text{Brugg}}}{\varepsilon_n} [W_3''(X)] + K = Q \quad (15)$$

Since  $V_i(\tau)$  is a function of  $\tau$  only and  $W_i(X)$  is a function of  $X$  only,  $A$ ,  $P$ , and  $Q$  are constants. The solutions for the dimensionless equations in each region after SOV and considering the BCs and initial condition (IC) can thus be obtained. Since there are no time-varying BCs or source terms,  $V_i(\tau)$  are identically zero:

$$V_1(\tau) = V_2(\tau) = V_3(\tau) = 0 \quad (16)$$

This allows the  $W_i(X)$  terms to be determined as (where  $B = \text{Brugg}$ ):

$$W_1(X) = \left[ \frac{X^2}{2} \varepsilon_p^{1-B} \right] + Z \quad (17)$$

$$W_2(X) = \left[ \frac{X p \varepsilon_p}{\varepsilon_s^B} \right] + \left[ p^2 \varepsilon_p \left( \frac{1}{2 \varepsilon_p^B} - \frac{1}{\varepsilon_s^B} \right) \right] + Z \quad (18)$$

$$W_3(X) = -K \varepsilon_n^{1-B} \left[ \frac{X^2}{2} - X - \frac{q^2}{2} + q \right] + \left[ \frac{p^2 \varepsilon_p^{1-B}}{2} \right] + \left[ \frac{(pq - p^2) \varepsilon_p}{\varepsilon_s^B} \right] + Z \quad (19)$$

Expressions (17)–(19) illustrate the steady state solution. Note that the forms for  $W_i(X)$  as presented above are for the case that the pore wall flux,  $J_i$ , is constant across the electrode. If the fluxes of lithium are allowed to change with position only,  $W_i(X)$  would have to be modified. Furthermore, if these fluxes are allowed to vary with time, the form of both  $V_i(\tau)$  and  $W_i(X)$  would be adjusted. However, if  $J_i$  is a function of both time and space, this analysis may not be valid, if the representation of  $J_i$  is not of an appropriate form.

The steady state solutions given above in Eqs. 17–19 represent the concentration profile when the competing effects of the Fickian diffusion due to the concentration gradient, and the ion migration, due to current flow, are in balance. In this dimensionless form, the rate of discharge is irrelevant, while the solutions are functions of  $K$ , the ratio of the current densities in the negative and positive electrodes. Increasing  $K$  has the effect of increasing the flux of lithium in the negative electrode relative to the positive electrode. However, it is not possible to adjust the relative fluxes independently of other factors. This ratio is given as

$$K = \frac{l_p \varepsilon_p}{l_n \varepsilon_n} = \frac{p \varepsilon_p}{(1 - q) \varepsilon_n} \quad (20)$$

Thus modifying  $K$  can only be achieved by adjusting one or more of those design parameters which would have other effects on the behavior of the system. For example, the diffusion resistance in the electrodes would change.

Furthermore, the transient expressions,  $U_1(X, \tau)$ , can be found from Eq. 12:

$$U_1(X, \tau) = \sum_{n=1}^{\infty} \left[ A_{1n} \left[ \cos \left( \alpha_n X \varepsilon_p^{\frac{1-B}{2}} \right) \right] \left[ \exp(-\alpha_n^2 \tau) \right] \right] \quad (21)$$

$$\begin{aligned} U_2(X, \tau) &= \sum_{n=1}^{\infty} \left[ \left[ A_{2n} \cos \left( \alpha_n X \varepsilon_s^{\frac{1-B}{2}} \right) + B_{2n} \sin \left( \alpha_n X \varepsilon_s^{\frac{1-B}{2}} \right) \right] \right. \\ &\quad \left. \times \exp(-\alpha_n^2 \tau) \right] \\ &= \sum_{n=1}^{\infty} \left[ \left[ E_{2n} \cos \left( \alpha_n X \varepsilon_s^{\frac{1-B}{2}} + \beta_n \right) \right] \exp(-\alpha_n^2 \tau) \right] \end{aligned} \quad (22)$$

$$U_3(X, \tau) = \sum_{n=1}^{\infty} \left[ A_{3n} \left[ \cos \left( \alpha_n (1-X) \varepsilon_n^{\frac{1-B}{2}} \right) \right] \left[ \exp(-\alpha_n^2 \tau) \right] \right] \quad (23)$$

where  $Z$  is a constant of integration, and  $\alpha_n$  and  $\beta_n$  are the eigenvalues, which are determined by satisfying the flux BCs at the region interfaces. Preserving the continuity at the interfaces, we solve  $A_{1n}$ ,  $A_{3n}$ ,  $E_{2n}$  in terms of a single constant  $A_n$ .

$$\begin{aligned} &\frac{A_{1n}}{\cos \left( \alpha_n p \varepsilon_s^{\frac{1-B}{2}} + \beta_n \right) \cos \left( \alpha_n (1-q) \varepsilon_n^{\frac{1-B}{2}} \right)} \\ &= \frac{E_{2n}}{\cos \left( \alpha_n p \varepsilon_p^{\frac{1-B}{2}} \right) \cos \left( \alpha_n (1-q) \varepsilon_n^{\frac{1-B}{2}} \right)} \\ &= \frac{A_{3n}}{\cos \left( \alpha_n q \varepsilon_s^{\frac{1-B}{2}} + \beta_n \right) \cos \left( \alpha_n p \varepsilon_p^{\frac{1-B}{2}} \right)} = A_n \end{aligned} \quad (24)$$

We now apply the terms determined in Eqs. 16–24 to the assumed form in Eq. 8 to complete the full series solution.

$$\begin{aligned} C_1(X, \tau) &= J_p \left\{ \sum_{n=1}^{\infty} \left[ A_n \left( \cos \frac{\alpha_n X}{\left( \frac{\varepsilon_p^B}{\varepsilon_p} \right)^{1/2}} \right) \cos \left( \alpha_n p \varepsilon_s^{\frac{1-B}{2}} + \beta_n \right) \right. \right. \\ &\quad \left. \left. \times \cos \left( \alpha_n (1-q) \varepsilon_n^{\frac{1-B}{2}} \right) \left( \exp(-\alpha_n^2 \tau) \right) \right] \right\} \\ &\quad + \left[ \left( \frac{J_p X^2}{2 \left( \frac{\varepsilon_p^B}{\varepsilon_p} \right)} \right) \right] + J_p Z + 1 \end{aligned} \quad (25)$$

$$\begin{aligned} C_2(X, \tau) &= J_p \left\{ \sum_{n=1}^{\infty} \left[ \left( A_n \cos \left( \frac{\alpha_n X}{\left( \frac{\varepsilon_s^B}{\varepsilon_s} \right)^{1/2}} + \beta_n \right) \right) \cos \left( \alpha_n p \varepsilon_p^{\frac{1-B}{2}} \right) \right. \right. \\ &\quad \left. \left. \times \cos \left( \alpha_n (1-q) \varepsilon_n^{\frac{1-B}{2}} \right) \left( \exp(-\alpha_n^2 \tau) \right) \right] \right\} \\ &\quad + \left[ \left( \frac{J_p p}{\left( \frac{\varepsilon_s^B}{\varepsilon_p} \right)} \right) X \right] + \left[ \left( \frac{J_p p^2}{\left( \frac{\varepsilon_p^B}{\varepsilon_p} \right)} \right) - \left[ \left( \frac{J_p p^2}{\left( \frac{\varepsilon_s^B}{\varepsilon_p} \right)} \right) \right] \right] \\ &\quad + J_p Z + 1 \end{aligned} \quad (26)$$

$$\begin{aligned} C_3(X, \tau) &= J_p \left\{ \sum_{n=1}^{\infty} \left[ \left( A_n \cos \frac{\alpha_n (1-X)}{\left( \frac{\varepsilon_n^B}{\varepsilon_n} \right)^{1/2}} \right) \right. \right. \\ &\quad \left. \left. \times \cos \left( \alpha_n q \varepsilon_s^{\frac{1-B}{2}} + \beta_n \right) \cos \left( \alpha_n p \varepsilon_p^{\frac{1-B}{2}} \right) \left( \exp(-\alpha_n^2 \tau) \right) \right] \right\} \\ &\quad + \left[ \left( -\frac{J_n}{\left( \frac{\varepsilon_n^B}{\varepsilon_n} \right)} \right) \left( \frac{X^2}{2} - X - \frac{q^2}{2} + q \right) \right] \\ &\quad + \left[ \left( \frac{J_p p^2}{\left( \frac{\varepsilon_p^B}{\varepsilon_p} \right)} \right) + \left[ \left( \frac{J_p (pq - p^2)}{\left( \frac{\varepsilon_s^B}{\varepsilon_p} \right)} \right) \right] \right] \\ &\quad + J_p Z + 1 \end{aligned} \quad (27)$$

There is no variation in the integration constant,  $Z$ , the series coefficients,  $A_n$ , or the eigenvalues,  $\alpha_n$  and  $\beta_n$ , once they are found for a given set of system parameters and are not affected by the rate of discharge. In order to obtain the integration constant  $Z$  as well as  $A_n$ , we apply the concept of averaging and orthogonality. At  $\tau = 0$ ,  $C_1 = C_2 = C_3 = 0$ . Since there is not a net gain or loss of lithium ions in the system throughout operation, the average concentration remains constant at all times

$$0 = \left( \varepsilon_p \int_0^p C_1 dX \right) + \left( \varepsilon_s \int_p^q C_2 dX \right) + \left( \varepsilon_n \int_q^1 C_3 dX \right) \quad (28)$$

Using Eq. 28 and solving for  $Z$ , we obtain the following expression:

$$Z = \frac{\left( -\varepsilon_p^{2-B} p^3 + 3\varepsilon_s^{1-B} p^3 - 3\varepsilon_s^{1-B} p^3 \varepsilon_p + 6\varepsilon_s^{1-B} p^2 \varepsilon_p q - 3\varepsilon_s^{1-B} p^2 q - 3p \varepsilon_s^{1-B} \varepsilon_p q^2 + 6\varepsilon_n \varepsilon_s^{-B} p q^2 \varepsilon_p \right. \\ \left. - 6 \frac{\varepsilon_n^{2-B} p \varepsilon_p q^2}{(1-q) \varepsilon_n} + 6\varepsilon_n \varepsilon_s^{-B} p^2 \varepsilon_p + 2 \frac{\varepsilon_n^{2-B} p \varepsilon_p q^3}{(1-q) \varepsilon_n} + 3\varepsilon_n \varepsilon_p^{1-B} p^2 q - 6\varepsilon_n \varepsilon_s^{-B} p^2 \varepsilon_p q \right. \\ \left. - 2 \frac{\varepsilon_n^{2-B} p \varepsilon_p}{(1-q) \varepsilon_n} - 6\varepsilon_n \varepsilon_s^{-B} p q \varepsilon_p + 6 \frac{\varepsilon_n^{2-B} p \varepsilon_p q}{(1-q) \varepsilon_n} - 3\varepsilon_n \varepsilon_p^{1-B} p^2 \right)}{6(\varepsilon_p p - \varepsilon_s p + \varepsilon_s q + \varepsilon_n - \varepsilon_n q)} \quad (29)$$

In order to determine the series coefficients, we use the following weight functions to preserve orthogonality

$$f_1 = \cos\left(\frac{\alpha_n X}{\left(\frac{\varepsilon_p}{\varepsilon_n}\right)^{1/2}}\right) \cos\left(\alpha_n p \varepsilon_s^{\frac{1-B}{2}} + \beta_n\right) \cos\left(\alpha_n (1-q) \varepsilon_n^{\frac{1-B}{2}}\right) \quad (30)$$

$$f_2 = \cos\left(\frac{\alpha_n X}{\left(\frac{\varepsilon_s}{\varepsilon_n}\right)^{1/2}} + \beta_n\right) \cos\left(\alpha_n p \varepsilon_p^{\frac{1-B}{2}}\right) \cos\left(\alpha_n (1-q) \varepsilon_n^{\frac{1-B}{2}}\right) \quad (31)$$

$$f_3 = \cos\left(\frac{\alpha_n (1-X)}{\left(\frac{\varepsilon_n}{\varepsilon_p}\right)^{1/2}}\right) \cos\left(\alpha_n q \varepsilon_s^{\frac{1-B}{2}} + \beta_n\right) \cos\left(\alpha_n p \varepsilon_p^{\frac{1-B}{2}}\right) \quad (32)$$

We have, at  $\tau = 0$ :

$$0 = \left(\varepsilon_p \int_0^p C_1 f_1 dX\right) + \left(\varepsilon_s \int_p^q C_2 f_2 dX\right) + \left(\varepsilon_n \int_q^1 C_3 f_3 dX\right) \quad (33)$$

Using Eqs. 30–33 and solving for  $A_n$ , we get:

#### 4 Extensions to varying and nonlinear parameters

The solutions presented above only address a simplified model in which all parameters are constant; this disregards the many nonlinear phenomena that arise in electrochemical systems. The solution procedure described above provides the basis of an approximate solution technique for nonlinear scenarios. The series form of solution (25–27) is again used; however, the obtained solution is approximate, unlike the linear case which gives an exact solution. This then provides a semi-analytical solution similar to the Galerkin methods that have been used in other areas of chemical engineering [25, 26].

As an initial proof of concept, the model was modified to include a nonlinear diffusion coefficient based on the work of Valøen and Reimers [27] and adjusted for the dimensionless concentration used. Also, an additional factor was included so that the value of the diffusivity at the initial concentration is the same as the constant diffusivity used in the remainder of the article. The nonlinear diffusion term used is:

$$D_{\text{nonlinear}} = 311709 \times 10^{\left(-4.65 - \frac{54}{64 - 1.230C(X,\tau)} - 0.0541C(X,\tau)\right)} \quad (35)$$

With the governing equations modified slightly and given as

$$\frac{\partial C_1}{\partial \tau} = \varepsilon_p^{\text{Brugg}-1} \frac{\partial}{\partial X} \left[ D_{\text{nonlinear}} \frac{\partial C_1}{\partial X} \right] - 1 \quad (0 \leq X \leq p, \text{ positive electrode}) \quad (36)$$

$$A_n = \frac{\varepsilon_s^{1/2+1/2B} \left( \frac{2 \sin\left(\alpha_n p \varepsilon_s^{1/2-1/2B} + \beta_n\right) \cos\left(\alpha_n \varepsilon_n^{1/2-1/2B} (1-q)\right) \cos\left(\alpha_n p \varepsilon_p^{1/2-1/2B}\right)}{\sin\left(\alpha_n q \varepsilon_s^{1/2-1/2B} + \beta_n\right) \cos\left(\alpha_n \varepsilon_n^{1/2-1/2B} (1-q)\right) \cos\left(\alpha_n p \varepsilon_p^{1/2-1/2B}\right) \varepsilon_p p} + 2 \frac{\sin\left(\alpha_n q \varepsilon_s^{1/2-1/2B} + \beta_n\right) \cos\left(\alpha_n \varepsilon_n^{1/2-1/2B} (1-q)\right) \cos\left(\alpha_n p \varepsilon_p^{1/2-1/2B}\right) \varepsilon_p p}{\varepsilon_n (1-q)} \right)}{\alpha_n^3 \left( (q-p) \left( \cos\left(\alpha_n \varepsilon_n^{1/2-1/2B} (1-q)\right) \right)^2 \left( \cos\left(\alpha_n p \varepsilon_p^{1/2-1/2B}\right) \right)^2 \varepsilon_s \right.} \quad (34)$$

$$\left. + \varepsilon_n \left( \cos\left(\alpha_n p \varepsilon_p^{1/2-1/2B}\right) \right)^2 \left( \cos\left(\alpha_n q \varepsilon_s^{1/2-1/2B} + \beta_n\right) \right)^2 (1-q) \right. \\ \left. + \left( \cos\left(\alpha_n \varepsilon_n^{1/2-1/2B} (1-q)\right) \right)^2 \left( \cos\left(\alpha_n p \varepsilon_s^{1/2-1/2B} + \beta_n\right) \right)^2 (p \varepsilon_p) \right)$$

The final solutions for concentrations in the respective regions depend only on the system parameters (i.e.,  $L, p, q, \varepsilon$ , Brugg) and is independent of the applied current ( $i_{\text{app}}, J_p$ ).

$$\frac{\partial C_2}{\partial \tau} = \varepsilon_s^{\text{Brugg}-1} \frac{\partial}{\partial X} \left[ D_{\text{nonlinear}} \frac{\partial C_2}{\partial X} \right] \quad (p \leq X \leq q, \text{ separator}) \quad (37)$$

$$\frac{\partial C_3}{\partial \tau} = \varepsilon_n^{\text{Brugg}-1} \frac{\partial}{\partial X} \left[ D_{\text{nonlinear}} \frac{\partial C_3}{\partial X} \right] + K \quad (38)$$

( $q \leq X \leq 1$ , negative electrode)

In order to solve for the concentration profiles, we begin using the eigenfunctions determined previously, and the form of the equations will be the same as given in Eqs. 25–27. However, for the nonlinear example, the coefficients  $A_n$  cannot be determined analytically and are time dependent (due to the changing diffusivity). The integration constant is the same as in (29).

This form ensures that the BCs are satisfied, as well as conserving mass. If simple trial functions (e.g., sine, cosine) were used, at least thrice the number of terms and equations would be needed, and the BCs would have to be supplied independently. In order to choose the coefficients of the eigenfunctions,  $A_n$ , that best approximates the exact solution, the method of orthogonal collocation can be used. Collocation methods are well established and thorough analysis can be found in the literature [20, 28, 29]. Collocation determines the coefficients by requiring that the governing equations be satisfied at specific points in the domain. These points can be arbitrarily chosen, but provide the most accurate numerical solution when the points are chosen as zeros of a set of orthogonal polynomials called the Jacobi polynomials [20, 28, 29]. Typically, a greater number of terms results in better accuracy, but the number of collocation points used must be equal to the number of terms in order to have enough equations to determine the coefficients.

For the problem presented here, the domain has been scaled to range from 0 to 1. This makes choosing the collocation points convenient, as the zeros for the Jacobi polynomials are on the interval 0 to 1. However, the cathode ranges from 0 to  $p$ , the separator from  $p$  to  $q$ , and the anode from  $q$  to 1. This complicates the procedure slightly, as each region is subject to a different governing equation as well different eigenfunctions and approximate forms for the concentrations. Therefore, the region in which each collocation point is located must be considered. However, it is not necessary that each region be represented by the same number of points. The coefficients to be determined are the same for each region, so including additional points in any region potentially improve the accuracy in all regions, and fewer terms are required than if the three regions were treated individually. Alternatively, all the three regions can be scaled from 0 to 1 as illustrated elsewhere for ease of coding and to better control in which region the node points are located [20].

## 5 Results and discussion

The main advantage of the obtained solutions is that one can obtain the variations in concentration with respect to

time in terms of system parameters using an algorithmic procedure. The analytical results obtained are useful to predict the eigenfunctions for electrolyte concentrations which could be extended for inclusion into efficient reformulated models for the entire battery using porous electrode theory [19] and isothermal models [16] even at high rates of discharge. The value of  $A_n$  is independent of  $i_{\text{app}}$ , as can be seen in expression (34), and only depends on system parameters such as  $p$ ,  $q$ ,  $\varepsilon$ , and Brugg. This allows us to study the effect of applied current on concentration profiles without calculating  $A_n$  every time. A key advantage of analytical solutions is their ability to provide simple insights of the effects of varying parameters, without repeated numerical simulations.

In order to validate the analytical solution developed here, the predicted concentration profiles were compared to a numerical solution. The method of lines was used find a solution to serve as a benchmark since it is well established in the literature as a method to solve partial differential equations [30]. Equations 1–3 were discretized in the spatial coordinate (i.e., in  $x$ ) using standard finite difference formulations, using 50 interior node points in the electrodes and 30 interior node points in the separator. Including the boundary points, this results in a system of 130 ordinary differential equations (ODEs). These ODEs can be solved simultaneously using efficient initial value problem (IVP) solvers, such as *dsolve* from Maple [31] or FORTRAN solvers such as DASKR or DASSL [32]. For a more complicated problem, the discretized system may be composed of differential algebraic equations (DAEs), which requires proper initialization to ensure consistent ICs of the algebraic variables before *dsolve* or DASKR could be applied [33].

An example will be presented using the base parameters given in Table 1. Importantly, Table 2 shows the convergence of the coefficient terms in the infinite series solution. Figure 2 shows the variations in the concentration as a function of distance for different rates of discharge at different times for these parameters. The rates presented are for a 1C and 2C rate, which corresponds to a dimensionless current of  $J_p = 0.25$  and  $J_p = 0.50$ , respectively, for this system. Also note that dimensionless concentration

**Table 1** Base system parameters

System parameters	
$p$	0.414
$q$	0.544
$B$	4
$\varepsilon_p$	0.385
$\varepsilon_s$	0.724
$\varepsilon_n$	0.485



determined from the above equations is independent of the applied current. Therefore, the dimensionless concentration shown in the figures is  $\bar{C}_i = (c_i/c_0)$ , rather than the  $C_i = ((c_i/c_0) - 1)/Jp$  used in the calculation, to show the effect

**Table 2** Convergence of  $A_n$  for base case

$n$	$\alpha_n$	$\beta_n$	$A_n$
1	0.96209	−1.77089	13.01783
2	1.75123	−1.1996	0.08203
3	2.8153	−2.7633	0.1057
4	3.7329	−2.4712	0.02493
5	4.611	−4.0506	0.01742
6	5.8596	−3.7556	0.04866
7	6.4117	−5.3206	0.006861
8	7.9512	−4.82215	0.009684
9	8.2886	−6.267	0.002264
10	9.836	−5.8522	0.00231

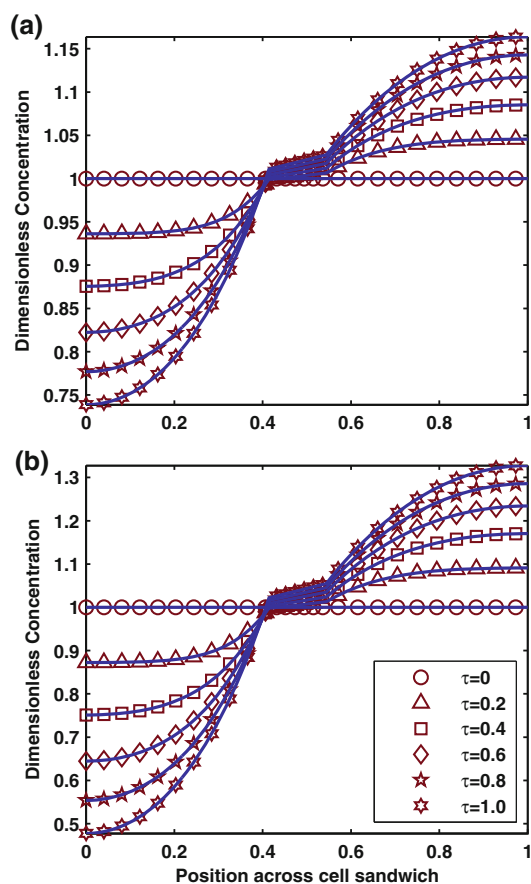


**Fig. 2** Comparison of the concentration profile as determined with the analytical solution to the profile as determined with numerical methods at **a** 1C and **b** 2C. The *solid lines* represent the analytical solution, while the *symbols* show the numerical solution using finite difference

of modifying the applied current on the concentration profile.

It can be seen that the analytical solution agrees well with the solution determined using numerical methods. Furthermore, once the analytical solution is found, determining the concentration at any point at any time is computationally trivial and can be done without computing values at points which are not of interest. In contrast, solving the problem numerically requires a procedure to be developed that is more computationally expensive. It is typically not possible to solve for the objective variable at a specific time and location without doing a step-by-step procedure that requires the computation of points which may not be of interest. For this reason, there is limited meaning when comparing the computational time of the two different methodologies.

Also we have the concentration as a function of time at the region interfaces within the battery (Fig. 3). Note that the concentration increases as we move from the positive end (cathode) of the battery to the negative end (anode) of the battery during discharge as lithium is transferred across the cell. Figure 3 shows that the battery reaches a steady state profile at which point the competing mass transfer effects of migration (due to the potential effects) and diffusion due to the concentration gradient are in balance. The mass transfer limit is reached in case of high-current rates and the diffusion coefficient falls down for higher Brugg's coefficient. This is shown by the predicted concentration going to zero in Fig. 4 when a 3C rate is applied.

The parameters given in Table 1 can be adjusted to match a wide range battery designs. This will affect the coefficients and eigenvalues used in the model. Table 3

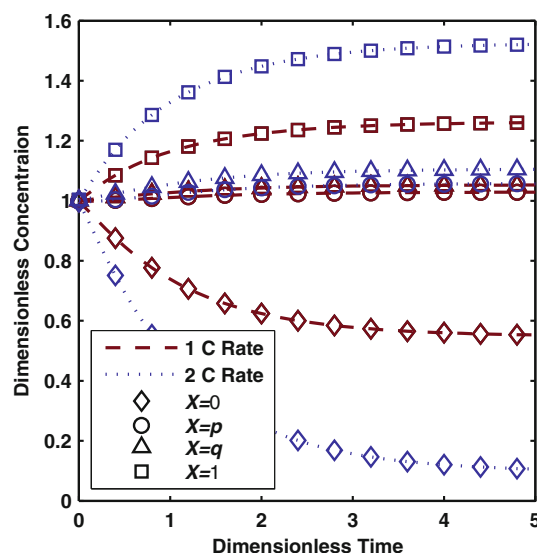


**Fig. 3** Comparison of concentration values at  $X = 0$ ,  $X = p$ ,  $X = q$ , and  $X = 1$ , for 1C (*dashed line*) and 2C (*dotted line*) rates of discharge under base conditions

shows an alternative set of parameters used in which a symmetrical battery is modeled. That is, when  $l_n = l_p$  and  $\varepsilon_n = \varepsilon_p$ . The resulting eigenvalues and coefficients shown in Table 4 are interesting, in that only the odd terms are nonzero. The model allows examination of the effect of modifying the design parameters on the concentration profile. Figure 5 shows the concentration profile for a 1C rate using the modified porosity parameters given in Table 5. A comparison of Figs. 2a and 5 shows that a decrease in porosity of a region (negative region in our case) leads to a greater concentration gradient, whereas increase in porosity (of the positive region) flattens the

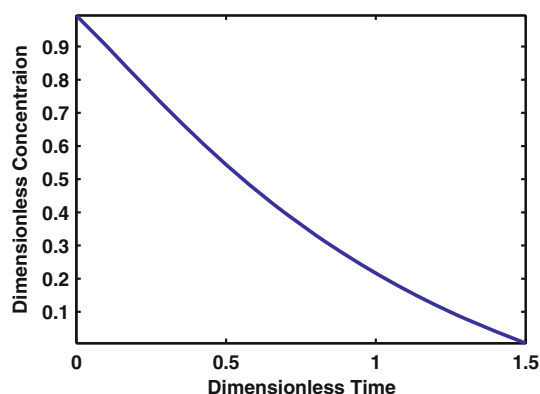


**Fig. 4** Concentration profile at  $X = 0$  for at 3C for base conditions

**Table 3** Parameters for symmetric design

System parameters	
$p$	0.4
$q$	0.6
$B$	4
$\varepsilon_p$	0.5
$\varepsilon_s$	0.724
$\varepsilon_n$	0.5

**Table 4** Case of  $\varepsilon_p = \varepsilon_n$  and  $l_p = l_n$  where even  $A_n$ 's go to zero

$n$	$\alpha_n$	$\beta_n$	$A_n$
1	1.31278	0.505295	40.67375
2	2.125727	-1.72532	$1.43 \times 10^{-15}$
3	3.913899	-1.60587	$1.57 \times 10^{-1}$
4	4.530191	-3.67687	$1.06 \times 10^{-14}$
5	6.415702	-3.63643	$9.93 \times 10^{-3}$
6	7.096382	-5.75969	$-2.25 \times 10^{-14}$
7	8.676729	-5.47156	$8.60 \times 10^{-4}$
8	9.716541	-4.74472	$4.02 \times 10^{-9}$
9	10.74072	-7.14677	$-4.86 \times 10^{-4}$
10	12.33599	-6.87076	$2.76 \times 10^{-14}$

concentration profile in that region. Thus, a lower  $\nabla c_i$  will be obtained by increasing the porosity of both the regions thereby reducing the mass transfer limitations.

The addition of the nonlinear diffusion coefficient provides a small but noticeable change from base conditions. In the analytical solutions, the nonlinearity has the effect of modifying the exponential decay of the linear transient solution; the coefficients,  $A_n$ , describe the (non-exponential) time evolution in the nonlinear case. In the linear case, the function coefficients implicitly decrease exponentially to a steady state value of zero. However, there is no requirement that the coefficients for the nonlinear case converge to a steady state value of zero, though they will converge to non-zero values. Table 6 shows the coefficient values,  $A_n$ , for the constant diffusion case and the nonlinear diffusion case at the start of simulation and for steady state conditions. In addition, note that using the analytical solution is important for spectral methods because a single coefficient,  $A_n$ , allows the profiles to be tracked in all the three regions.

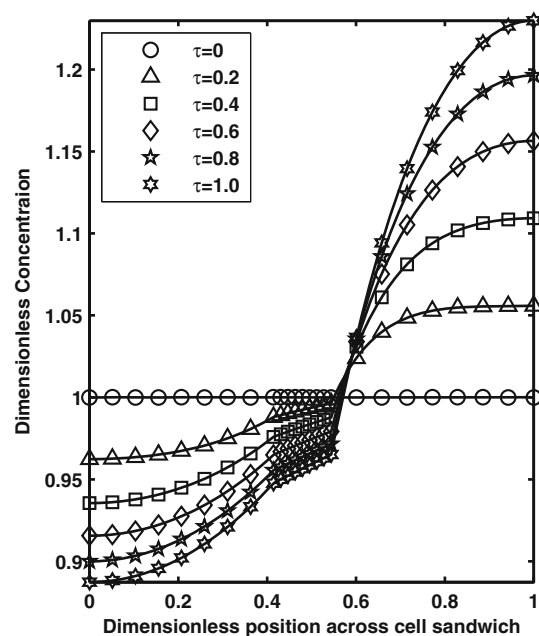


**Fig. 5** Concentration profile for modified porosity case at 1C

**Table 5** Parameters for modified porosity case

System parameters	
$p$	0.414
$q$	0.544
$B$	4
$\varepsilon_p$	0.6
$\varepsilon_s$	0.5
$\varepsilon_n$	0.4



**Table 6** Comparison of coefficients for constant diffusion and non-linear diffusion examples at the beginning of discharge and at steady state

Coefficient	Initial values		Steady state values	
	Constant diffusion	Nonlinear diffusion	Constant diffusion	Nonlinear diffusion
$A_1$	13.02	13.02	0	−0.4598
$A_2$	0.08202	0.08154	0	−0.04527
$A_3$	0.1057	0.1046	0	−0.07249
$A_4$	0.02493	0.02240	0	0.01630
$A_5$	0.01742	0.01250	0	$9.776 \times 10^{-3}$
$A_6$	0.04860	0.02268	0	0.03019
$A_7$	$6.861 \times 10^{-3}$	$-1.232 \times 10^{-4}$	0	0.01675

Figure 6 shows the concentration profile across the cell sandwich at various times for a 1C rate discharge when a nonlinear diffusion coefficient is used. This shows the concentration as calculated using collocation approach using the eigenfunctions as determined for the linear case. For comparison, a full-order finite difference solution is also presented. The primary advantage of using collocation on the eigenfunctions is the increase in computational efficiency. The finite difference solution used 125 node points requiring 125 nonlinear DAEs to be solved simultaneously. Conversely, the collocation approach can arrive at a reasonable approximation when using as few as seven terms and achieves better convergence as more terms are included. Figure 6a shows the concentration profile at different times, while Fig. 6b shows the residuals relative to the finite difference case. As the zeros of the Jacobi polynomials are used to determine the location of the collocation points used, it is possible that one of the three regions will not be represented by a single node point. For example, when eight node points are used, none are located within the separator. Interestingly, this does not seem to be detrimental to the convergence of the final solution, as can be seen in Fig. 6b. This is possible because the same coefficients are utilized in each region, while the continuity BCs are enforced by the form of the equations used. Therefore, the improved accuracy gained by additional node points in the positive and negative electrodes translates to improved convergence in the separator as well. It is worth noting that the positive electrode is the most difficult region to accurately simulate, as can be seen in Fig. 6, which shows the largest residuals are realized in the cathode.

## 6 Conclusions and summary

In this article, an analytical solution was obtained for the transient response of electrolyte concentration in lithium-ion batteries using the method of SOV. The method was efficient in obtaining relevant constants independent of current density. From the different plots, it can be

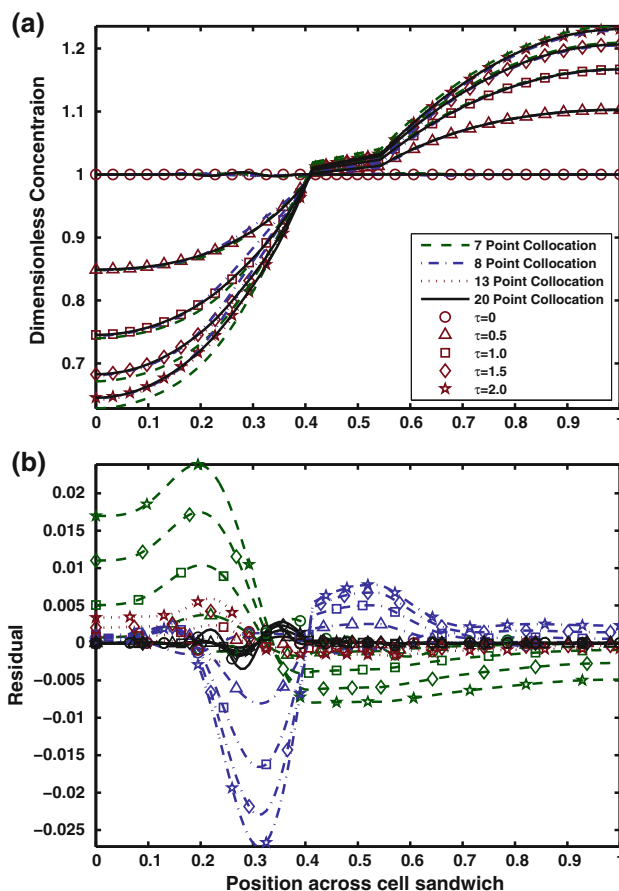


**Fig. 6** **a** Concentration profile across a battery with nonlinear diffusion as calculated using a finite difference method and the collocation method. **b** The residual of the collocation solutions with respect to finite difference

concluded that the concentration of Li-ion increases as we move from cathode to the anode during discharge. This variation is dependent on the design parameters, such as electrode porosity, as well as the operating applied current. In the case of higher discharge rates, a rapid depletion of Li-ion concentration occurs in the positive electrode, while a corresponding increase is observed in the negative

electrode. Collocation was used to simulate the same model subject to a nonlinear diffusion coefficient, since such a system cannot be solved analytically. The eigenfunctions that were found for linear problem were then applied as trial functions in the collocation solutions with time varying coefficients. This provided a quick and accurate simulation of a more complicated model.

The SOV technique presented here for the electrolyte diffusion of lithium-ion batteries can be used to model the other variables of interest that arise in battery operation, such as solid phase diffusion and potential fields. Ultimately, it is possible that the eigenfunctions and eigenvalues developed in such works could be implemented into a full battery model to allow for efficient numerical simulation. These eigenvalues would be applied in a manner similar to the non-linear diffusion coefficient discussed above. Similar attempts with slightly less optimal polynomial forms (in which each region was treated independently) have been attempted by our group in the past [16, 20], which will benefit more using the expressions developed in this article.

Furthermore, we believe that a similar analytical approach could be applied to a number of engineering models to improve computational efficiency. A number of models, ranging from heat transfer problems to reaction–diffusion models, are governed by mathematically similar equations to those presented here. Furthermore, the eigenvalues and eigenfunctions could be applied in a numerical manner to account for a variety of possible non-linearities in addition to the non-linear diffusion coefficient explained here. For example, temperature-dependent parameters could be incorporated into the model using Arrhenius relations for non-isothermal systems.

**Acknowledgments** The authors are thankful for the partial financial support of this work by the National Science Foundation (CBET-0828002, CBET-1008692, CBET-1004929), the United States government, McDonnell Academy Global Energy and Environment Partnership (MAGEEP) at Washington University in St. Louis.

## Appendix

The governing equations are given in dimensional form as:

$$\varepsilon_p \frac{\partial c_1}{\partial t} = D_{\text{eff},p} \frac{\partial^2 c_1}{\partial x^2} + a_p(1 - t_+)j_p \quad 0 \leq x \leq l_p \quad (39)$$

$$\varepsilon_s \frac{\partial c_2}{\partial t} = D_{\text{eff},s} \frac{\partial^2 c_2}{\partial x^2} \quad l_p \leq x \leq l_s + l_p \quad (40)$$

$$\varepsilon_n \frac{\partial c_3}{\partial t} = D_{\text{eff},n} \frac{\partial^2 c_3}{\partial x^2} + a_n(1 - t_+)j_n \quad l_p + l_s \leq x \leq l_n + l_s \quad (41)$$

With BCs determined from continuity of concentration and mass flux given as:

$$-D_{\text{eff},p} \frac{\partial c_1}{\partial x} = 0 \quad \text{at } x = 0, \quad -D_{\text{eff},n} \frac{\partial c_3}{\partial x} = 0 \quad \text{at } x = l_p + l_s + l_n \quad (42)$$

$$\begin{aligned} -D_{\text{eff},p} \frac{\partial c_1}{\partial x} &= -D_{\text{eff},s} \frac{\partial c_2}{\partial x} \quad \text{at } x = l_p, \\ -D_{\text{eff},s} \frac{\partial c_2}{\partial x} &= -D_{\text{eff},n} \frac{\partial c_3}{\partial x} \quad \text{at } x = l_p + l_s \end{aligned} \quad (43)$$

$$c_1(x, t) = c_2(x, t) \quad \text{at } x = l_p, \quad c_2(x, t) = c_3(x, t) \quad \text{at } x = l_p + l_s \quad (44)$$

With IC is given as:

$$c_1(x, 0) = c_2(x, 0) = c_3(x, 0) = c_0(x) \quad (45)$$

For this study, the pore wall flux in the electrode is assumed to be constant across space and time. In order to maintain a charge balance, the ionic fluxes in the positive and negative electrodes are not necessarily identical in magnitude, but scaled according to the electrode thickness and specific surface area. This leads to the following relations for the pore wall flux:

$$j_p = -\frac{i_{\text{app}}}{a_p F l_p} \quad (46)$$

$$j_n = +\frac{i_{\text{app}}}{a_n F l_n} \quad (47)$$

The diffusion coefficients at the respective electrodes are expressed in terms of the Bruggeman coefficient and porosity within each electrode.

$$D_{\text{eff},i} = D \varepsilon_i^{\text{Brugg}} \quad \text{for } i = p, s, n \quad (48)$$

The following dimensionless variables are used in order to transform the above equations to dimensionless form and to ensure that the solution is solved in terms of the system parameters ( $l_p, l_s, l_n, p, q, \varepsilon_p, \varepsilon_s, \varepsilon_n$ ):

$$C_i = \left( \frac{c_i}{c_0} - 1 \right) / Jp \quad \text{for } i = 1, 2, 3 \quad (49)$$

$$p = \frac{l_p}{L}, \quad q = \frac{l_p + l_s}{L} \quad (50)$$

$$\tau = \frac{Dt}{L^2} \quad (51)$$

$$X = \frac{x}{L} \quad (52)$$

$$J_i = \frac{i_{\text{app}}(1 - t_+)L^2}{\varepsilon_i D c_0 l_i F} \quad \text{for } i = p, n \quad (53)$$

$$K = \frac{J_n}{J_p} \quad (54)$$

where

$$L = l_p + l_s + l_n \quad (55)$$

## References

1. Gomadam PM, Weidner JW, Dougal RA, White RE (2002) *J Power Sources* 110:267
2. Doyle M, Fuller TF, Newman J (1993) *J Electrochem Soc* 140:1526
3. Doyle M, Newman J, Gozdz AS, Schmutz CN, Tarascon JM (1996) *J Electrochem Soc* 143:1890
4. Doyle M, Newman J (1997) *J Appl Electrochem* 27:846
5. Newman J, Tiedemann W (1975) *AIChE J* 21:25
6. Botte GG, Subramanian VR, White RE (2000) *Electrochim Acta* 45:2595
7. Arora P, Doyle M, Gozdz AS, White RE, Newman J (2000) *J Power Sources* 88:219
8. Atlung S, West K, Jacobsen T (1979) *J Electrochem Soc* 126:1311
9. Fuller TF, Doyle M, Newman J (1994) *J Electrochem Soc* 141:982
10. Fuller TF, Doyle M, Newman J (1994) *J Electrochem Soc* 141:1
11. Ning G, White RE, Popov BN (2006) *Electrochim Acta* 51:2012
12. Ramadass P, Haran B, Gomadam PM, White R, Popov BN (2004) *J Electrochem Soc* 151:A196
13. Ramadass P, Haran B, White R, Popov BN (2003) *J Power Sources* 123:230
14. Cai L, White RE (2009) *J Electrochem Soc* 156:A154
15. Cai L, White RE (2010) *J Electrochem Soc* 157:A1188
16. Subramanian VR, Boovaragavan V, Ramadesigan V, Arabandi M (2009) *J Electrochem Soc* 156:A260
17. Forman JC, Bashash S, Stein JL, Fathy HK (2011) *J Electrochem Soc* 158:A93
18. Subramanian VR, Boovaragavan V, Diwakar VD (2007) *Electrochem Solid State* 10:A255
19. Boovaragavan V, Harinipriya S, Subramanian VR (2008) *J Power Sources* 183:361
20. Northrop PWC, Ramadesigan V, De S, Subramanian VR (2011) *J Electrochem Soc* 158:A1461
21. Subramanian VR, White RE (2001) *J Power Sources* 96:385
22. Hashim Ali SA, Hussin A, Arof AK (2002) *J Fizik Malaysia* 23:145
23. Crank J (1983) *The mathematics of diffusion*. Oxford University Press, Oxford
24. Thomas KE, Newman J (2003) *J Electrochem Soc* 150:A176
25. Marchant TR (2002) *P Roy Soc Lond A* 458:873
26. Thornton AW, Marchant TR (2008) *Chem Eng Sci* 63:495
27. Valøen LO, Reimers JN (2005) *J Electrochem Soc* 152:A882
28. Carey GF, Finlayson BA (1975) *Chem Eng Sci* 30:587
29. Villadsen J, Michelsen ML (1978) *Solution of differential equation models by polynomial approximation*. Prentice-Hall, Englewood Cliffs
30. Schiesser WE (1991) *The numerical method of lines: integration of partial differential equations*. Academic Press, New York
31. <http://www.maplesoft.com/Products/Maple>. Accessed 21 Feb 2012
32. Brenan KE, Campbell SL, Campbell SLV, Petzold LR (1996) *Numerical solution of initial-value problems in differential-algebraic equations*. Society for Industrial and Applied Mathematics, Philadelphia
33. Methekar RN, Ramadesigan V, Pirkle JC, Subramanian VR (2011) *Comput Chem Eng* 35:2227